Journal of Colloid and Interface Science 484 (2016) 263–269

Contents lists available at ScienceDirect

Journal of Colloid and Interface Science

journal homepage: www.elsevier.com/locate/jcis

Shell thickness matters! Energy transfer and rectification study of Au/ZnO core/shell nanoparticles

Krishna Kanta Haldar [a,*], Tapasi Sen [b]

[a] Centre for Chemical Science, School of Basic and Applied Science, Central University of Punjab, City Campus, Mansa Road, Bathinda 151001, Punjab, India
[b] Institute of Nano Science & Technology, Mohali 160062, Punjab, India

GRAPHICAL ABSTRACT

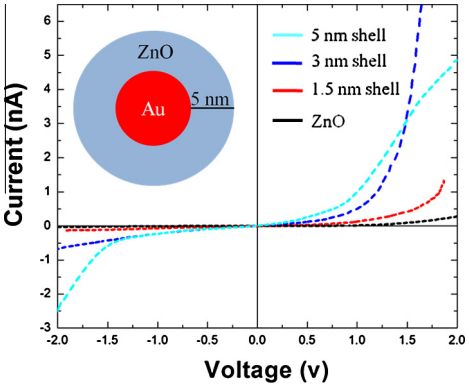

ARTICLE INFO

Article history:
Received 9 June 2016
Revised 25 August 2016
Accepted 3 September 2016
Available online 6 September 2016

Keywords:
FRET
Core–shell nanoparticle
Dye
Spectroscopy
Rectification

ABSTRACT

In the present study we report the influence of shell thickness on fluorescence resonance energy transfer between Au/ZnO core-shell nanoparticles and Rhodamine 6G dye by steady-state and time-resolved spectroscopy and rectification behaviours. Au/ZnO core-shell nanoparticles with different shell thickness were synthesized in aqueous solution by chemically depositing zinc oxide on gold nanoparticles surface. A pronounced effect on the photoluminescence (PL) intensity and shortening of the decay time of the dye in presence of Au/ZnO core-shell nanoparticles is observed. The calculated energy transfer efficiencies from dye to Au/ZnO are 62.5%, 79.2%, 53.6% and 46.7% for 1.5 nm, 3 nm, 5 nm and 8 nm thickness of shell, respectively. Using FRET process, the calculated distances (r) are 117.8, 113.2 Å 129.9 Å and 136.7 Å for 1.5 nm, 3 nm, 5 nm and 8 nm thick Au/ZnO core-shell nanoparticles, respectively. The distances (d) between the donor and acceptor are 71.0, 57.8, 76.2 and 81.6 Å for 1.5 nm, 3 nm, 5 nm and 8 nm thick core-shell Au/ZnO nanoparticles, respectively, using the efficiency of surface energy transfer (SET). The current-voltage (I-V) curve of hybrid Au/ZnO clearly exhibits a rectifying nature and represents the *n*-type Schottky diode characteristics with a typical turn-on voltage of between 0.6 and 1.3 V. It was found that the rectifying ratio increases from 20 to 90 with decreasing the thickness of the shell from 5 nm to 3 nm and with shell thickness of 8 nm, electrical transport through the core-shell is similar to what is observed with pure ZnO samples nanoparticles. The results indicated that the Au/ZnO core-shell nanoparticles with an average shell thickness of 3 nm exhibited the maximum energy transfer efficiencies (79.2%) and rectification (rectifying ratio 90).

* Corresponding author.
E-mail addresses: cskkh@cup.ac.in, krishnakanta.haldar@gmail.com (K.K. Haldar).

http://dx.doi.org/10.1016/j.jcis.2016.09.006
0021-9797/

1. Introduction

The design and architecture of programmable metal–semiconductor nanostructures with excellent optoelectronic properties from metal and semiconductor building blocks with nanoscale dimensions have recently been a key aim due to their central roles in the fabrication of electronic, optical, and optoelectronic nanodevices [1]. Metal-semiconductor core-shell nanocomposites have received significant attention because they provide a new system with unique and tailored properties which are entirely different from the physical and chemical properties of metal and semiconductor nanoparticles [2–5]. In addition, the semiconductor shell can protect the metal core (higher oxidation potentials) from chemical poisoning as exposed to the surrounding medium [6]. More importantly, the presence of the metal/semiconductor interface may promote effective charge carrier transfers to favour charge separation and subsequent photocatalysis [7]. In metal-coated semiconductor nanoparticles, the charge transfer between semiconductor and metal nanoparticles can be controlled by the size-dependent capacitance of metal nanoparticles. In recent years, important progress has been made in solution-phase synthesis of core-shell-type Ag/TiO_2, Au/TiO_2, Au/SnO_2, Fe_2O_3/Au for potential applications [5,8–10]. Using the aqueous-phase synthetic method, Au/SiO_2 [11–13], Cu_2S/Au [14], InAs/Au [15], and Au/CdS [16] heterojunctions were also acquired.

A significant attention has been paid recently in the field of quantum dot (QD)-based fluorescence energy transfer to find out potential applications in the areas of luminescence tagging, imaging, medical diagnostics, multiplexing and most recently as biosensors [17–25]. This interest stems from their tunable electronic structure, narrow emission and broad excitation spectra and the large size of QD compared to organic dyes [17]. Recently, metal nanoparticles based surface energy transfer provides a new paradigm for design of optical based molecular ruler for long distance measurement. According to Persson–Lang model, the exact form of dipole-surface energy transfer rate is given by

$$k_{SET} = \frac{1}{\tau_D}\left(\frac{d_0}{d}\right)^4 \quad (1)$$

where τ_D is the lifetime of the donor in the absence of the acceptor, d is the distance between the donor and acceptor, and d_0 is the characteristic distance at which a dye will display equal probabilities for energy transfer and spontaneous emission. The energy transfer between dye and Au/ZnO and Au/SnO_2 core-shell nanoparticles were studied by Patra et al. [26,27]. Banin et al. [28] have demonstrated the effects of the dimensionality and shape of Nanoparticles (NPs) acting as donors on the Fluorescence resonance energy transfer (FRET) to dye molecules chemically conjugated to the NP surface, acting as multiple acceptors.

To the best of our knowledge, there is no study on the rectifying nature of Au/ZnO core-shell core-shell nanoparticles. In this study we will focus on the synthesis of water soluble Au/ZnO core-shell nanoparticles having different shell thicknesses and investigate the rectification properties of Au/ZnO core-shell nanoparticles having different shell thicknesses and propose an approach of nanocrystal solids through the intra-particle charge transfer. In this communication, we also study the energy transfer from Rhodamine 6G dye to such nanoparticles by steady state and time-resolved spectroscopy. Such Au/ZnO multifunctional nanoparticles should have great potentials for optical-based molecular ruler because such core-shell nanoparticle shows high electronic storage capacity at Au nanoparticle. Au/ZnO core-shell nanostructure has been chosen as a model system to study coupling effects between strongly confined metal and semiconductor phases.

2. Result and discussion

Here, water soluble and stable Au/ZnO core-shell nanocomposite having four different shell thicknesses were prepared by using our previous method with some modifications [26]. For this particular procedure, Au nanoparticles were about ~7 nm in diameter, with nearly spherical shape. The detail synthesis procedure of different shell thicknesses Au/ZnO core-shell nanocrystals has been described in supporting information. The crystallinity of the gold, ZnO nanoparticles and different shellthickness of Au/ZnO core-shell nanocomposite were characterized by the powder X-ray diffraction (XRD) studies. As shown in Fig. 1a, the Au nanoparticles demonstrate a highly crystalline structure and the peak at 38° is predominated in the XRD spectra, which is indexed to the metallic Au (1 1 1) crystal plane (JCPDS 98-000-0230). From the diffraction pattern of Au@ZnO core-shell nanoparticles, The diffraction peak at 36° (Fig. 1f) is indexed to (1 0 1) plane and the remaining peaks in all the specimens are indexed to be hexagonal structure of ZnO (JCPSD 36-1451). Moreover, the intensities of the peak at 38° for gold gradually quench and the diffraction peaks for ZnO systematically enhance observably with the increasing shell-thickness from 1.5 nm to 8 nm, which is consistent with the variation in shell-thickness of ZnO coated on Au nanoparticles in the Au/ZnO core-shell nanocomposite nanostructure (see Fig. 1).

Fig. 2a–d reveals a wide view of the TEM images showing the core-shell type heterostructures, where Au is covered preferably by ZnO with roughly sphere shape. They could easily assemble together to form a 2D structure when dropped on the carbon-supported copper grid with an appropriate concentration. Without size sorting, the spherical Au/ZnO core-shell nanocrystals obtained here showed good monodispersity with the existence of well-resolved lattice planes. The Au/ZnO core-shell nanoparticles possessed a highly crystalline structure. The low resolution TEM images of the four different shell-thickness of Au/ZnO core-shell nanostructure clearly indicate the formation of Au/ZnO core-shell composite structure. To further confirm the Au/ZnO core-shell heterostructure; we have studied the high resolution transmission electron microscope (HRTEM). Fig. 3 shows the typical TEM, HRTEM and fast Fourier transform (FFT) of the prepared Au/ZnO core-shell nanoparticles having four different shell thicknesses. As shown in Fig. 3a and b, Au/ZnO nanostructure images by TEM and HRTEM confirms 1.5 and 3 nm shell thickness, respectively.

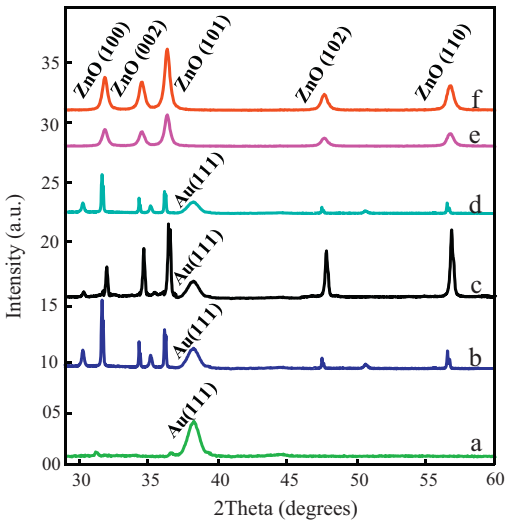

Fig. 1. Powder X-ray diffraction patterns of (a) Au, (b) Au@ZnO (1.5 nm shell), (c) Au@ZnO (3 nm shell), (d) Au@ZnO (5 nm shell), (e) Au@ZnO (8 nm shell) and (f) ZnO nanoparticles.

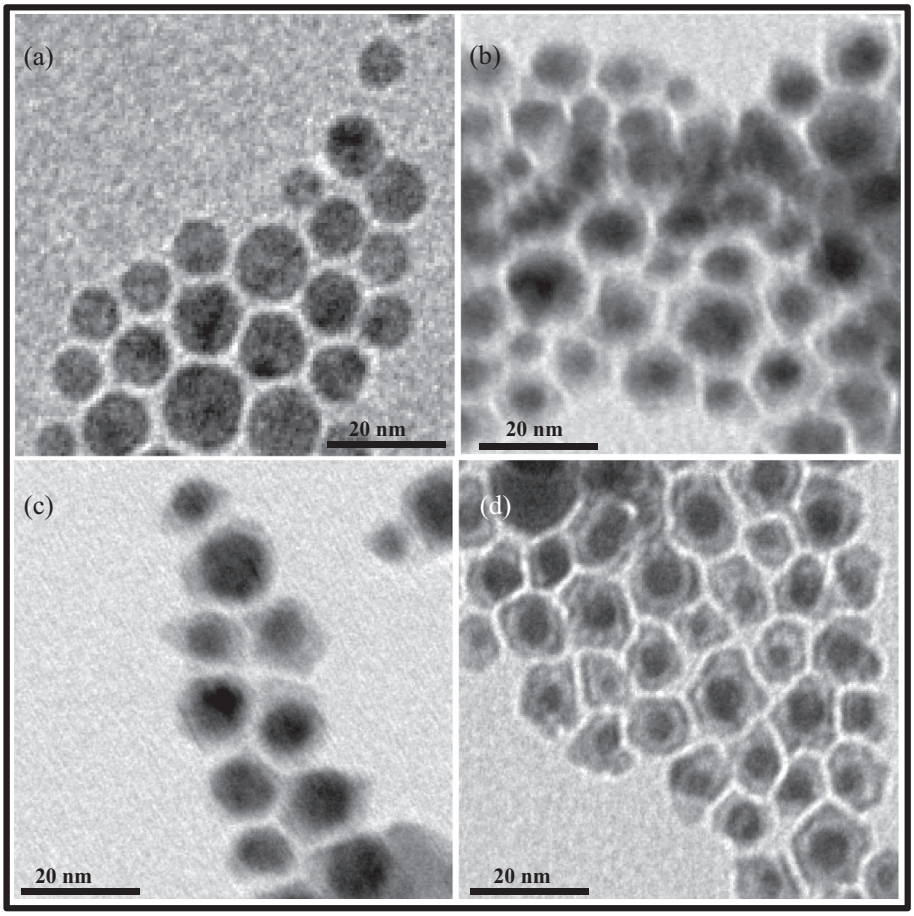

Fig. 2. TEM images of Au/ZnO nanostructures with 1.5 nm (a), 3 nm (b), 5 nm (c) and 8 nm (d) shell thickness, respectively.

HRTEM images were analyzed by FFT (Fig. 3c and d). Fig. 3e and f presents typical TEM and HRTEM image of a single core-shell structure 8 nm shell thickness Au/ZnO nanostructures where core Au and shell ZnO areas are marked to achieve the FFT of the selected area. Fig. 3g and h FFT from core areas and shell areas, respectively, of the HRTEM image presented in panel f. The dark contrast of the image is the Au, and the light contrast part is the ZnO. HRTEM and FFT images confirmed that the cubic (1 1 1) phase of the Au NPs were coated to the (1 0 1) plane of the hexagonal phase of the ZnO. TEM and typical HRTEM images of 5 nm shell thickness Au/ZnO core-shell heteronanostructures are shown in Fig. 3i, j and k shows the corresponding d-profile of ZnO shells. The calculated d-spacing (2.48 Å) suggests that the shell atom is ZnO and it is viewed along [1 0 1] direction. So, it is clearly seen from HRTEM that Au nanoparticle is coated with ZnO and the measured thickness of the shell are of 1.5 nm, 3 nm 5 nm and 8 nm, respectively.

The absorption spectra of pure Au and Au/ZnO core-shell nanoparticles with different thickness of shell are presented in Fig. 4. The absorption peaks centered at 521, 532, 543 nm, 548 nm and 556 nm are due to plasmon band for pure Au, 1.5 nm, 3 nm, 5 nm and 8 nm thick shell of Au/ZnO nanocomposite, respectively. The systematic shifting of the plasmonic peak of Au indicates the formation of Au/ZnO core-shell nanoparticles. Here, the surface plasmon band of Au are red shifted and the excitonic peak of ZnO are blue shifted which are consistent with the formation of four different shell thicknesses Au/ZnO core-shell nanostructure (plot c–f). Since the Fermi level of Au is more positive (E_F = 0.4 V vs NHE) than the conduction band energy of ZnO (E_{CB} = 0 V vs NHE at pH 7), the charge transfer from the excited ZnO to Au nanoparticles would be thermodynamically favorable. It indicates that more electrons are needed to raise Fermi level for higher capacitance value. It reveals that the shell thickness of core-shell nanoparticles controls the charge capacitance value. Furthermore, the primary ZnO particle size in Au/ZnO core-shell nanoparticles is smaller compared to pure ZnO NPs, which may also be one of the reasons behind the blue shift in absorption band of ZnO in Au/ZnO core-shell nanoparticles [29].

3. Steady state photoluminescence (PL) study

Fig. 5 depicts very good overlapping between the emission spectrum of aqueous solution of unbound R6G dye (pure) and the absorption spectrum of Au/ZnO nanoparticles containing R6G dye solution. The PL peak at 550 nm is due to R6G dye. The observed PL quenching efficiencies are 66.5% and 85.8% for Au/ZnO core-shell nanoparticles having 1.5 nm, 3 nm thick shells, respectively and it is 57.5% and 51.3% for 5 nm and 8 nm shellthickness Au/ZnO core-shell nanoparticles, respectively. The photoluminescence quenching of R6G dye in presence of Au/ZnO composites nanoparticles indicates that the energy transfer occurred from R6G dye to Au and Au/ZnO composites nanoparticles. To confirm the energy transfer process, we have study the time-resolved fluorescence spectra of R6G dye. The time-resolved fluorescence spectra of aqueous solution of pure R6G dye and in presence of Au/ZnO nanoparticles are shown in Fig. 6. The photoluminescence decay of aqueous solution of pure R6G dye (1 μM)

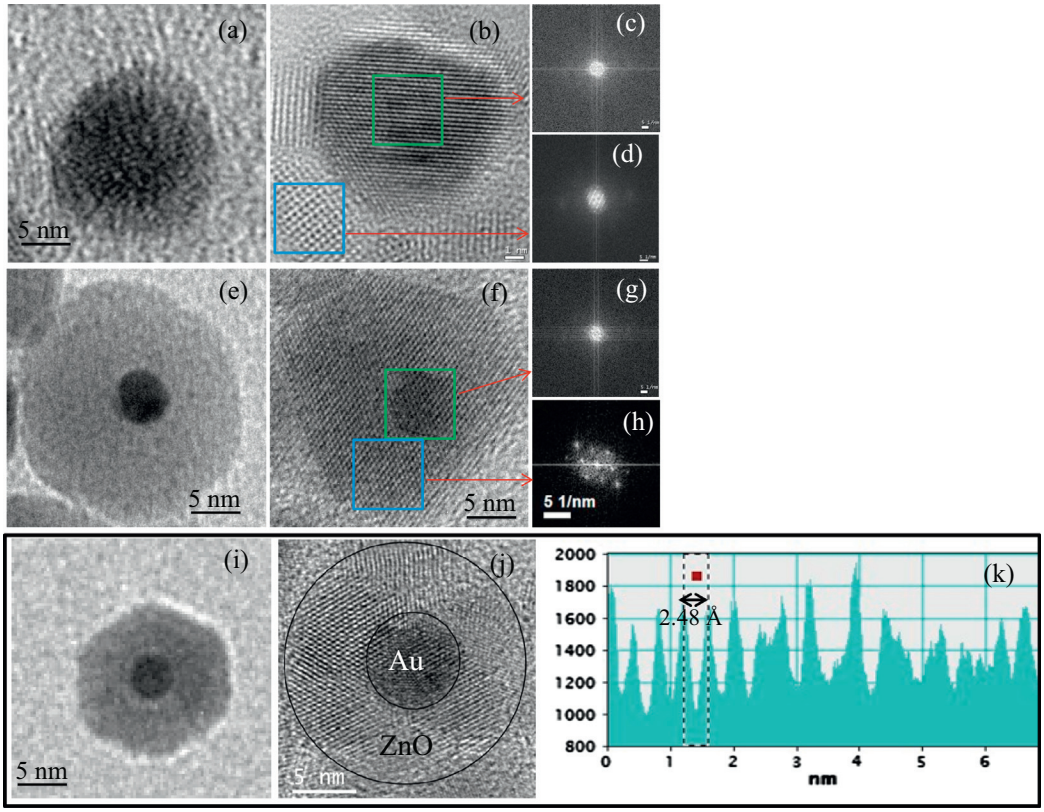

Fig. 3. (a) TEM images of 1.5 nm shell thickness Au/ZnO nanostructures, (b) HRTEM images of 3 nm shell thickness Au/ZnO core/shell nanostructures (c and d) the corresponding FFT of Au core and ZnO shell, respectivly. (e) TEM images of 8 nm shell thickness Au/ZnO heteronanostructures, (f) typical HRTEM image where core Au and shell ZnO areas are marked to achieve the FFT of the selected area. (g and h) FFT from core areas and shell areas, respectively, of the HRTEM image presented in panel f. (i and j) TEM and typical HRTEM images of 5 nm shell thickness Au/ZnO heteronanostructures and (k) shows the corresponding d-profile of ZnO shells.

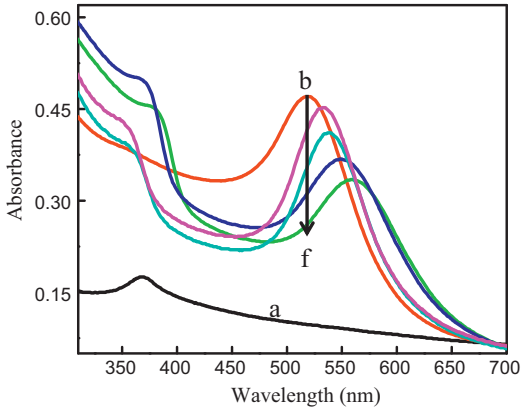

Fig. 4. UV–vis spectra of (a) ZnO (black line), (b) Au nanoparticles (red line), (c) Au@ZnO (1.5 nm shell, magenta line), (d) Au@ZnO (3 nm shell, cyan line), (e) Au@ZnO (5 nm shell, blue line) and (f) Au@ZnO (8 nm shell green line). (For interpretation of the references to color in this figure legend, the reader is referred to the web version of this article.)

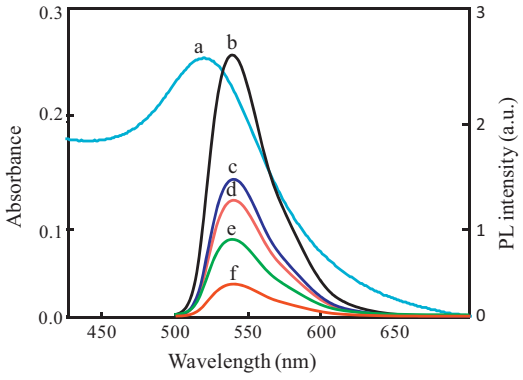

Fig. 5. Absorption spectrum of pure Au NPs (a) and photoluminescence (PL) spectra of (b) Rhodamine 6G dye solution, (c) Au@ZnO (8 nm) core-shell nanoparticle and R6G, (d) Au@ZnO (5 nm) core-shell nanoparticle and R6G, (e) Au@ZnO (1.5 nm) core-shell nanoparticle and R6G and (f) Au@ZnO (3 nm) core-shell with R6G.

without Au/ZnO is single exponential and the decay time is 3.91 ns, which is for unbound dye molecules. However, the fluorescence decay spectra of dye in presence of Au/ZnO nanoparticles having different shell thicknesses are fitted by using tri-exponential function. In presence of 1.5 nm thick shell Au/ZnO nanoparticles, the decay components of dye are 3.39 ns (25.7%), 0.362 ns (27.1%) and 93.5 ps (47.2%) and the average decay time is 1.46 ns. A drastic shortening of life time of R6G dye was observed in presence of Au/ZnO core-shell nanocomposite of 3 nm thick shell. The decay components are 3.16 ns (4.2%), 0.267 ns (41.7%) and 94.2 ps (64.1%) and the average decay time is 0.872 ns. Again the life time of the core-shell nanoparticles increases upon increasing the thickness of shell. In presence of an Au/ZnO core-shell nanocomposite of 5 and 8 nm thick shell nanoparticles, the components of dye are 3.48 (49.6%), 0.41(13.5%), and 98.7 ps (37.1%) and 3.69 ns (53.5%), 0.355 ns (23.1%) and 106.3 ps (23.4), respectively and the average decay time is 1.96 ns and 2.08 ns, respectively (Table 1). The slow component is due to unbound dye molecules and fast components are attributed to bound dye molecules with Au/ZnO nanoparticles. The shortening of lifetime of dye in presence of Au/ZnO nanoparticles

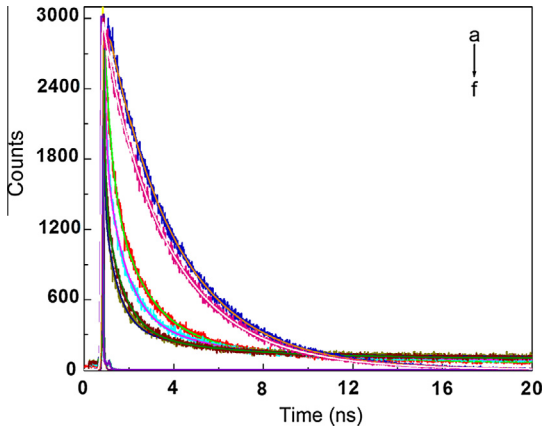

Fig. 6. The decay curves of (a) Rhodamine 6G dye solution, (b) R6G with Au@ZnO (8 nm) core-shell, (c) R6G with Au@ZnO (5 nm) core-shell, (e) R6G with Au@ZnO (1.5 nm) core-shell and (f) R6G with Au@ZnO (3 nm) core-shell nanoparticles, respectively.

confirms the energy transfer from dye to Au/ZnO nanoparticles. The calculated energy transfer efficiencies from dye to nanoparticles are found to be 62.6%, and 79.2% for 1.5 nm and 3 nm thick shells of Au/ZnO nanocomposite, respectively, which is thickness dependent but energy transfer from dye to Au/ZnO nanoparticles again decreases upon increasing the shell thickness and it is 49.8% and 46.7% for 5 nm and 8 nm thick shell Au/ZnO nanoparticles, respectivly. It clearly indicates that transfer efficiencies from dye to Au/ZnO core-shell nanoparticles is shell-thickness dependent and increases with increasing the shell thickness and after getting optimum it decreases with increasing the shell thickness. It is interesting to note that the non-radiative decay rates are 4.1×10^8, 9.82×10^8, 3.95×10^8 and 3.81×10^8 $s^{-1}$for Au/ZnO nanoparticles having thicknesses of 1.5 nm, 3 nm, 5 nm and 8 nm, respectively (Table 2). More pronounced effect on nonradiative decay rate suggests that the PL quenching of dye is mainly due to nonradiative decay channel without any significant modification of the radiative rate which confirms the resonant energy transfer process from R6G dye molecule to Au/ZnO core-shell nanoparticles [26].

Both Fluorescence resonance energy transfer (FRET) and surface energy transfer (SET) methods are used to estimate the distance between donor and acceptor [30,31]. It is already reported that FRET based method is restricted [24] on the upper limit of only 80 Å because the energy transfer becomes too weak to be useful. Furthermore, we estimate the distance between donor and acceptor by using surface energy transfer (SET) method. We estimate the d_o value by using Persson model [31]

$$d_0 = \left(\frac{0.225 c^3 \Phi_{dye}}{\omega_{dye}^2 \omega_F k_F} \right)^{1/4} \quad (2)$$

where d_o is the distance at which a dye will display equal probabilities for energy transfer and spontaneous emission. ϕ_{dye} is the quantum efficiency of dye, the frequency of the donor electronic transition (ω), and the Fermi frequency (ω_F), and Fermi wave vector (k_F) of the metal [26]. The d_0 value was calculated using $\phi_{dye} = 0.92$, $\omega = 3.6 \times 10^{15}$ s^{-1}, $\omega_F = 8.4 \times 10^{15}$ s^{-1}, and $k_F = 1.2 \times 10^8$ cm^{-1}, and $c = 3 \times 10^{10}$ cm s^{-1}. The calculated d_0 value is 80.76 Å for Au/ZnO nanoparticles. The distances (d) between the donor and acceptor are 71.0, 57.8, 76.2 and 81.6 Å for 1.5 nm, 3 nm,5 nm and 8 nm thick core-shell Au/ZnO nanoparticles, respectively, using the efficiency of surface energy transfer (SET) which depends on the inverse fourth power of the distance of separations between donor and acceptor. As FRET based method is restricted on the upper limit of only 80 Å, therefore, we may suggest that the energy transfer from dye to Au/ZnO nanoparticles follows surface energy transfer (SET) process in the present study. The energy transfer process depends on the shell thickness of Au/ZnO core-shell nanoparticles which is an important finding in this study.

Table 2
Radiative and nonradiative decay rates of R6G dye in presence of Au/ZnO core-shell nanoparticles having four different shell thicknesses.

System	Radiative rate (s^{-1})	Non-radiative rate (s^{-1})
Au/ZnO (1.5 nm) + R6G Dye	1.76×10^8	4.10×10^8
Au/ZnO (3 nm) + R6G Dye	2.20×10^8	9.82×10^8
Au/ZnO (5 nm) + R6G Dye	1.84×10^8	3.95×10^8
Au/ZnO (8 nm) + R6G Dye	1.98×10^8	3.81×10^8

4. Current-voltage characterisation

Electrical characteristics of different junctions and their components were characterized with a Pt/Ir tip of a scanning tunneling microscope (STM, Nanosurf easyScan2) controller in noncontact (tunneling) mode under ambient conditions. Here, the tip was approached till a preset current value (at a particular voltage) was achieved. A topographic image of the surface was recorded before current-voltage (I-V) characteristics were measured at different points on the film. Voltage was scanned toward both bias directions and at different sweep speeds. Hybrid Au/ZnO core-shell exhibits unique structural characteristics and is an interesting system to know how electrons behave when they are transported through a core-shell junction. In order to judge the potentiality of forming functional devices using these core-shell nanocomposites, we have carried out an electrical study of the core-shell. The resulting current–voltage (I-V) curve of the device through the Au/ZnO hybrid core-shell with varying the thickness of the shell ZnO are shown in Fig. 7. The I-V characteristic curves of were measured in different point like "A" and "B" for Au@ZnO core-shell nanostructure of shell thickness 3 nm, are shown in the supporting information (Fig. S1). The I-V curve clearly exhibits a rectifying nature and represents the *n*-type Schottky diode characteristics of hybrid Au/ZnO (3 nm) with a typical turn-on voltage of between 0.6 and 1.3 V. The I-V characteristics of a junction determine its working condition governed by the role of charge carriers and the barrier. Schottky contacts are metal-semiconductor junctions which are valuable when high speed rectification is required where

Table 1
Time resolved fluorescence quenching studies of Rh6G in presence of Au/ZnO core-shell nanoparticles having four different shell thicknesses.

System	b_1 (%)	τ_1[a] (ps)	b_2 (%)	τ_2[a] (ns)	b_3 (%)	τ_3[a] (ns)	$\langle\tau\rangle$[a] = $\sum b_i \tau_i$ (ns)	χ^2	E (%)
Rh6G dye (1 μM)	–	–	–	–	100	3.91	3.91	1.06	–
Au @ZnO (1.5 nm) + Rh6G	47.2	93.5	27.1	0.362	25.7	3.39	1.46	1.08	62.6
Au @ZnO (3 nm) + Rh6G	64.1	94.2	41.7	0.267	4.2	3.16	0.872	1.09	79.2
Au @ZnO (5 nm) + Rh6G	37.1	98.7	13.5	0.410	49.6	3.48	1.96	1.07	53.6
Au @ZnO (8 nm) + Rh6G	23.4	106.3	23.1	0.355	53.5	3.69	2.08	1.10	46.7

[a] ±5% (error).

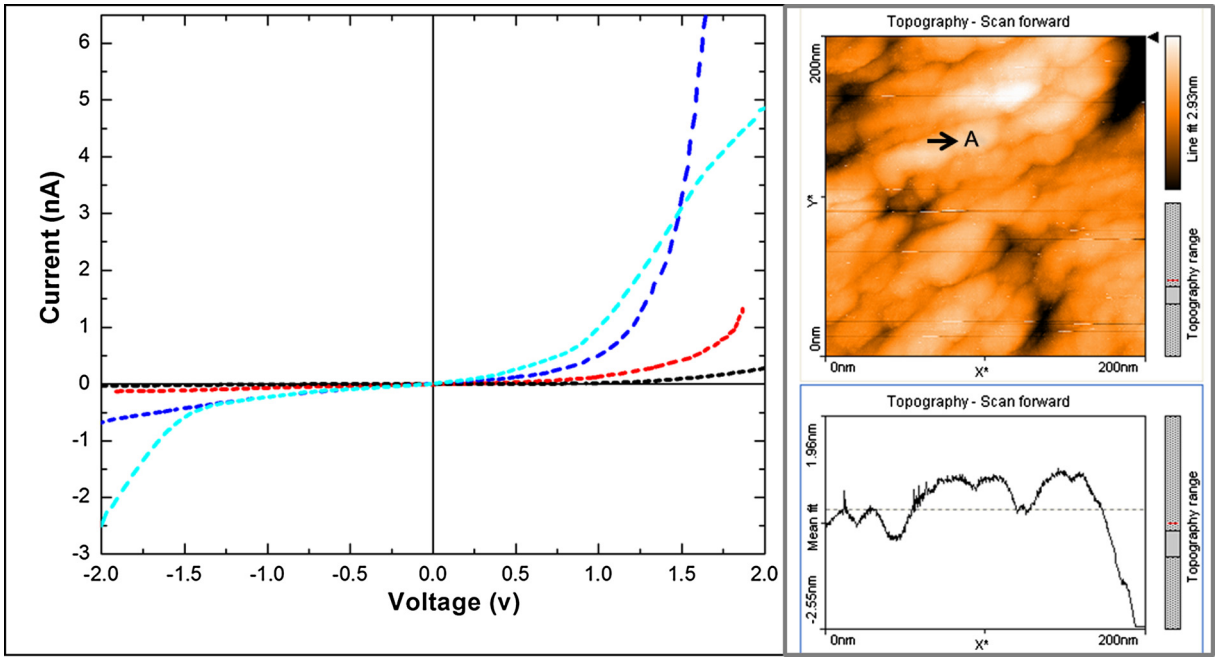

Fig. 7. I-V characteristic curves of (a) 1.5 nm (cyan), (b) 3 nm (blue) and (c) 5 nm (red) Au@ZnO core-shell nanostructure of shell thickness of, respectively, and (d) ZnO. I-V curves were recorded in regions "A" for Au@ZnO core-shell nanostructure of shell thickness 3 nm. (For interpretation of the references to color in this figure legend, the reader is referred to the web version of this article.)

as ohmic contacts are useful for non-rectifying operations. It is known that bulk- metal/ZnO junctions drives current relatively at higher bias voltage with respect to nano metal/ZnO junctions [32]. The plots exhibit rectification, with current flow being favorable from ZnO to Au ones. It is known that intrinsic ZnO is an *n*-type semiconductor with a work function of 4.45 eV and the work function of Au is 5.1 eV [32]. Thus, a Pt/Ir electrode is made to facilitate the electron flow from Au nanocrystals to the ZnO since the Fermi level of the ZnO nanoparticle is initially lower than that of the Au metal before the contact was made [27]. This process results in the formation of an electron depletion region at the surface of Au nanoparticles that corresponds to a Schottky barrier between the ZnO nanoparticles and Au Nanoparticles. The curve of pure ZnO is linear and symmetric, which is in agreement with their expected intrinsic properties and indicates the contact between nanoparticle and metal electrode is not responsible for the appreciable rectification [33]. The curves of Au/ZnO (1.5 nm shell) junction are highly nonlinear but slight asymmetric indicating a more metal-like behaviour. On the other hand, Au/ZnO (3 nm shell) core-shell intramolecular junction are highly nonlinear and asymmetric, exhibiting typical diode-like behaviour. When the forward bias voltage is 0.86 V, the current increases abruptly by order of 10^{-8} A. The current for the reverse bias condition is of the order of 10^{-10} A, much lower in magnitude than the threshold voltage for the forward bias condition. As the thickness of ZnO layer increases, the curves looks like typical pure ZnO samples (Fig. 7d). With shell thickness of 8 nm, electrical transport through the core-shell is similar to what is observed with pure ZnO samples. Stronger contributions to the electrical transport were observed between the shell thickness of 3 and 5 nm of Au/ZnO hybrid nanomaterials. Thus the rectifying ratio increases from 20 to 90 for Au/ZnO hybrid systems having 5 nm and 3 nm shell thicknesses, respectively. The high rectification ratio of 90 suggests good rectifying characteristics of the 3 nm shell thick Au/ZnO core-shell nanoparticles intramolecular junctions, providing a high performance nanoscale diode. Therefore, we can conclude the rectifying behaviour of the 3 nm thick shell Au/ZnO nanocomposite should be attributed to the intrinsic intramolecular junction of the hybrid nanoparticle.

5. Conclusion

In the present study, we have demonstrated the preparation of Au/ZnO core-shell nanoparticles with different shell thicknesses. We have analyzed and confirmed these core-shell nanostructures using high-resolution transmission electron microscope (HRTEM). The Au/ZnO core-shell nanoparticles of 3 nm thick shell exhibited significantly improved rectification performances as compared to that of pure ZnO NPs as well as other three different thickness core-shell. The rectifying ratio increases from 20 to 90 for 5 nm and 3 nm thick shell Au/ZnO hybrid nanocomposite, respectively. The high rectification ratio of 90 suggests good rectifying characteristics of the 3 nm shell thick Au/ZnO core-shell nanoparticles intramolecular junctions, providing a high performance nanoscale diode. The influence of shell thickness on energy transfer from R6G dye to Au/ZnO core-shell nanoparticles has also been studied. Such multifunctional nanoparticles should have great potentials for optical-based molecular rulers and it could pave the way for designing new electrical device for the application in electrical diode.

Acknowledgements

This work is financially supported by Central University of Punjab, Bathinda, India by its Research Seeds Grant.

Appendix A. Supplementary material

Details experimental and instrumental methods for Au/ZnO core-shell nanoparticles synthesis and characterization are available in supporting information. Supplementary data associated with this article can be found, in the online version, at http://dx.doi.org/10.1016/j.jcis.2016.09.006.

References

[1] X. Feng, G. Hu, J. Hu, Nanoscale 3 (2011) 2099–2117.
[2] T. Hirakawa, P.V. Kamat, J. Am. Chem. Soc. 127 (2005) 3928–3934.
[3] P.V. Kamat, J. Phys. Chem. C 111 (2007) 2834–2860.
[4] X. Wang, X. Kong, Yi. Yu, H.J. Zhang, Phys. Chem. C 111 (2007) 3836–3841.
[5] G. Oldfield, T. Ung, P. Mulvaney, Adv. Mater. 12 (2000) 1519–1522.
[6] V. Subramanian, E. Wolf, P.V. Kamat, J. Phys. Chem. B 105 (2001) 11439–11446.
[7] M. Jakob, H. Levanon, P.V. Kamat, Nano Lett. 3 (2003) 353–358.
[8] J. Li, D. Li, X. Hong, L. Wang, K. Zhao, J. Li, Y. Bai, T. Li, Chem. Commun. 8 (2004) 982–983.
[9] H. Sakai, T. Kanda, H. Shibata, T. Ohkuba, M. Abe, J. Am. Chem. Soc. 128 (2006) 4944–4945.
[10] J. Kim, D. Lee, J. Am. Chem. Soc. 129 (2007) 7706–7707.
[11] E. Mine, A. Yamada, Y. Kobayashi, M. Konno, L.M. Liz-Marzán, J. Colloid Interf. Sci. 264 (2003) 385–390.
[12] I.P. Santos, J. P_erez-Juste, L.M. Liz-Marz_an, Chem. Mater. 18 (2006) 2465–2467.
[13] Y. Lu, Y.D. Yin, Z.Y. Li, Y.N. Xia, Nano Lett. 2 (2002) 785–788.
[14] X.G. Wen, S.H. Yang, Nano Lett. 2 (2002) 451–454.
[15] T. Mokari, A. Aharoni, I. Popov, U. Banin, Angew. Chem. Int. Ed. 45 (2006) 8001–8005.
[16] W.T. Chen, T.T. Yang, Y.J. Hsu, Chem. Mater. 20 (2008) 7204–7206.
[17] I.L. Medintz, A.R. Clapp, H. Mattoussi, E.R. Goldman, B. Fisher, J.M. Mauro, Nat. Mater. 2 (2003) 630–638.
[18] A.R. Clapp, I.L. Medintz, B.R. Fisher, G.P. Anderson, H. Mattoussi, J. Am. Chem. Soc. 127 (2005) 1242–1250.
[19] T. Pons, I.L. Medintz, K.E. Sapsford, S. Higashiya, A.F. Grimes, D.S. English, H. Mattoussi, Nano Lett. 7 (2007) 3157–3164.
[20] H. Peng, L. Zhang, T.H.M. Kjallman, C. Soeller, J.T. Sejdic, J. Am. Chem. Soc. 129 (2007) 3048–3049.
[21] A. Boulesbaa, A. Issac, D. Stockwell, Z. Huang, J. Huang, J. Guo, T. Lian, J. Am. Chem. Soc. 129 (2007) 15132–15133.
[22] P.S. Chowdhury, P. Sen, A. Patra, Chem. Phys. Lett. 413 (2005) 311–314.
[23] D. Zhou, J.D. Piper, C. Abell, D. Klenerman, D.J. Kang, L. Ying, Chem. Commun. 38 (2005) 4807.
[24] S. Dayal, Y. Lou, A.C.S. Samia, J.C. Berli, M.E. Kenney, C. Burda, J. Am. Chem. Soc. 128 (2006) 13974–13975.
[25] S. Dayal, C. Burda, J. Am. Chem. Soc. 129 (2007) 7977–7981.
[26] K.K. Haldar, T. Sen, A. Patra, J. Phys. Chem. C 112 (2008) 11650–11656.
[27] K.K. Haldar, A. Patra, Chem. Phys. Lett. 462 (2008) 88–91.
[28] S. Halivni, A. Sitt, I. Hadar, U. Banin, ACS Nano 6 (2012) 2758–2765.
[29] S.M. Majhi, P. Rai, Y.T. Yu, ACS Appl. Mater. Interf. 7 (2015) 9462–9468.
[30] J.R. Lakowicz, Principles of Fluorescence Spectroscopy, third ed., Springer, New York, 2006.
[31] T. Sen, S. Sadhu, A. Patra, Appl. Phys. Lett. 91 (2007). 043104-1.
[32] K. Mohanta, A.J. Pal, Nanotechnology 20 (2009) 185203.
[33] S.JuS. Kim, S. Mohammadi, D.B. Janes, App. Phys. Lett. 92 (2008). 022104.